Structure–function analysis of LIV-1, the breast cancer-associated protein that belongs to a new subfamily of zinc transporters

Kathryn M. TAYLOR[1], Helen E. MORGAN, Andrea JOHNSON, Lisa J. HADLEY and Robert I. NICHOLSON

Tenovus Cancer Research Centre, Welsh School of Pharmacy, Cardiff University, Redwood Building, King Edward VII Avenue, Cardiff CF10 3XF, U.K.

The LIV-1 gene has been previously associated with oestrogen-positive breast cancer and its metastatic spread to the regional lymph nodes. We have investigated the protein product of this gene as a marker for disease progression of breast cancer. The protein sequence contains a potential metalloprotease motif (HEX**PH**E**H**EXGD), which fits the consensus sequence for the catalytic zinc-binding site motif of the zincin metalloproteases. This motif has identified a new subfamily of ZIP (Zrt-, Irt-like proteins) zinc transporters, which we have termed LZT (LIV-1 subfamily of ZIP zinc transporters). Expression of recombinant LIV-1 in Chinese-hamster ovary cells confirmed the prediction that LZT proteins can act as zinc-influx transporters. Zinc is essential for growth and zinc transporters have an important role in maintaining intracellular zinc homoeostasis, aberrations of which could lead to diseases such as cancer. This is the first report of the expression of a recombinant human LZT protein in mammalian cells. Recombinant LIV-1 locates to the plasma membrane, concentrated in lamellipodiae, similar to membrane-type metalloproteases. Examination of LIV-1 tissue expression located it mainly to hormonally controlled tissues with widespread expression in the brain. Interestingly, the LIV-1 sequence contains a strong PEST site and other potential degradation motifs, which, combined with our evidence that recombinant LIV-1 associates with ubiquitin, may explain the low-level expression of LIV-1. Combining the crucial role that zinc plays in cell growth and the proven role of metalloproteases in metastasis presents an exciting indication of how LIV-1 plays a role in breast cancer progression.

Key words: breast cancer, HEXXH, LIV-1, metalloprotease, zinc transporter, ZIP (Zrt-, Irt-like protein) transporter.

INTRODUCTION

LIV-1 has been identified as a novel gene whose expression is stimulated by oestrogen treatment of MCF-7 and ZR-75 breast cancer cells (4- and 8-fold respectively) [1]. Our investigation of LIV-1 expression in clinical breast-tumour populations reveals a significant association with oestrogen receptor status [2], a fact that also indicates the response of a patient to endocrine therapy [3]. Importantly, however, LIV-1 mRNA expression also shows a highly significant association with the spread of breast cancer to the regional lymph nodes [4], a relationship which is absent from other oestrogen-regulated genes (e.g. PR and pS2 [4]). In particular, LIV-1 associates with small (< 2 cm) oestrogen-receptor-positive tumours of which 92 % show lymph-node involvement. This increases the possibility that LIV-1 expression may be both a suitable prognostic marker for lymph-node involvement and also a key determinant of metastatic spread in steroid hormone receptor-positive disease.

LIV-1 has been shown to belong to a new subfamily of ZIP (Zrt-, Irt-like proteins) zinc transporters, now termed LZT (LIV-1 subfamily of ZIP zinc transporters) [5]. We have shown previously that these sequences, currently 36 from over 12 species [5], contain a novel potential metalloprotease motif [6] similar to that present in the MMPs (matrix metalloproteases), which have an important and well-documented role in metastasis [7].

Eukaryotes have many zinc transporters, which have now been implicated in the transport process, but all have not been fully characterized. The most researched transporters belonged either to the ZIP or the CDF (cation diffusion family) transporter families, as reviewed by Gaither and Eide [8]. ZIP transporters are situated either on the plasma membrane and act as zinc influx transporters or are situated on the intracellular membranes allowing them to mobilize stores from these structures. The ZIP family consists of at least 86 members and can be divided into four separate subfamilies [8].

There are at least 15 known human members of the ZIP-transporter superfamily [5], with one in ZIP subfamily I, three in ZIP subfamily II (hZIP1, hZIP2 and hZIP3), two in the gufa subfamily and nine in the LIV-1 subfamily. Previous studies in mammalian cells have indicated that both hZIP1 and hZIP2 are time, temperature- and concentration-dependent zinc uptake transporters [9,10]. The similarity of the LIV-1 sequence to that of the ZIP transporters suggests that the LIV-1 family may also have a similar role.

Zinc is essential for cell growth and is a co-factor for more than 300 enzymes, representing over 50 different enzyme classes [11]. Zinc is involved in protein, nucleic acid, carbohydrate and lipid metabolism, as well as in the control of gene transcription, growth, development and differentiation [12]. Not only can zinc deficiency be detrimental, causing stunted growth and serious metabolic disorders [13], excess of it can also be toxic to cells [14]. Zinc cannot passively diffuse cell membranes; therefore, specific zinc transporter proteins are required to transport zinc into cells. As zinc is essential for cell growth, membrane proteins capable of transporting zinc into cells will have a crucial role in maintaining the cellular balance between apoptosis and cell growth, aberrations of which could lead to cancer.

In the present study, we investigate the expression of recombinant LIV-1 protein, the first study of a human member of the LZT subfamily in mammalian cells. We have shown its

Abbreviations used: CHO, Chinese-hamster ovary; DAPI, 4,6-diamidino-2-phenylindole; DIC, differential interference contrast; MMP, matrix metalloprotease; PNGase F, peptide N-glycosidase F; TM, transmembrane; TNT, transcription/translation *in vitro*; TPEN, *N*,*N*,*N*′,*N*′-tetrakis-(2-pyridylmethyl) ethylenediamine; ZIP, Zrt-, Irt-like proteins; LZT, LIV-1 subfamily of ZIP zinc transporters.

[1] To whom correspondence should be addressed (e-mail Taylorkm@cardiff.ac.uk).

localization to the plasma membrane lamellipodiae, similar to the membrane-type metalloproteases, which have been linked to metastasis. We also show how the presence of LIV-1 imparts a novel zinc uptake activity on the cells, confirming its role as a zinc transporter. Therefore the combination of zinc-uptake ability and potential metalloprotease activity suggests a possible mechanism for the role of LIV-1 in breast cancer progression.

EXPERIMENTAL

LIV-1 RNA expression in human tissues

A multiple-tissue expression array (MTE™, BD Biosciences, Oxford, U.K.), containing polyadenylated RNA from 68 normal human tissues and eight cancer cell lines was hybridized with a 540 bp LIV-1-specific ^{32}P-labelled cDNA probe (138–678 bp) according to the manufacturer's instructions.

Computer prediction of the LIV-1 sequence

The computer prediction of LIV-1 secondary structure was achieved using the GCG [Wisconsin Package Version 9.0, Genetics Computer Group (GCG), Madison, WI, U.S.A.] package of software as well as SignalP [15] for signal peptide prediction, PESTFIND for potential PEST sites [16] and SAPS for statistical analysis of protein structure [17]. Potential transmembrane (TM) domains were identified using a combination of SOSUI [18], TMPred [19], SOPMA [20], HMMTOP [21], DAS [22] and PSORT [23].

Generation of LIV-1 cDNA construct

A LIV-1 PCR construct was generated using oligonucleotide primers (overlap with LIV-1 is underlined): 5′-CCCATCGGATCCGGCACAATGGCGAGGAAGTTATC-3′ (138–154 bp) and 5′-GAAATTTATACGAAACACGATTTTATG-3′ (2358–2384 bp), removing the stop sign to PCR-amplify clone pLIV-1-F1 (U41060) using 1 unit Biotaq DNA polymerase from Bioline (London, U.K.). The PCR parameters were 2 min at 94 °C, followed by 25 cycles of 1 min at 94 °C, 1 min at 55 °C, and 1 min at 72 °C, with a final extension for 30 min at 72 °C. The product was ligated to pcDNA3.1/V5-His-TOPO (Invitrogen, Paisley, U.K.), adding the V5 epitope (5 kDa in this vector), for 5 min at 25 °C. TOP10 One Shot cells were transformed and colonies were grown on ampicillin plates overnight at 37 °C before testing for insert and orientation by PCR. Constructs were validated by sequence analysis using the BigDye Terminator cycle sequencing ready reaction kit (Applied Biosystems, Warrington, Cheshire, U.K.) and an ABI Prism 377 DNA sequencer (Applied Biosystems).

Translation of LIV-1 *in vitro*

The LIV-1 pcDNA3.1/V5-His-TOPO construct was transcribed/translated *in vitro* (TNT), with or without the addition of canine pancreatic microsomal membranes (Promega, Chilworth, Southampton, U.K.), using the TNT quick-coupled Transcription/Translation system (TNT; Promega), according to the manufacturer's instructions. Samples were analysed by SDS/PAGE and detected with the Transcend system (Promega). The product was immunoprecipitated with 1 μg of mouse anti-ubiquitin antibody (StressGen Biotechnologies, San Diego, CA, U.S.A.) or 1 μg of mouse anti-V5 antibody (Invitrogen). Samples analysed by Western blotting were either probed with antibody or detected by horseradish peroxidase chemiluminescence using West Femto reagent (PerbioScience, Cheshire, U.K.).

Expression of recombinant LIV-1 in CHO (Chinese-hamster ovary) cells

CHO cells were maintained in minimal essential medium (Sigma) with 10 % (v/v) foetal calf serum, 4 mM glutamine, 20 μg/ml penicillin and streptomycin and 2.5 μg/ml fungizone in 5 % CO_2 at 37 °C. Cells were transfected with the relevant pcDNA3.1/V5-His-TOPO constructs using LIPOFECTAMINE™ 2000 (Invitrogen), according to the manufacturer's instructions. Briefly, 9×10^5 cells, grown on 60 mm dishes for 24 h, were transfected with 8.8 μg of DNA and 27.5 μl of reagent in antibiotic-free media. Sodium butyrate (3 mM) was added 14 h before harvest.

Engineering LIV-1 mutants for expression in insect cells

The same TOPO-TA cloning method was used to engineer two TM-deletion mutants for expression in Schneider S2 *Drosophila* cells as described above but with the pMT/V5-His TOPO vector (Invitrogen), producing a C-terminal V5 tag of 2.6 kDa, and the following oligonucleotides. Overlap with LIV-1 sequence is underlined, LIV-1 residue numbers for the mutated protein construct are shown in parentheses and an Express epitope, added at the 3′-end, in bold: M3A (1–716, deletion of TM VIII), CCCATC**CTTATCGTCATCGTCGTACAGATC**CCAGCGGCTACATCC. M3G (1–345, deletion of TM II–VIII), CCCATC**CTTATCGTCATCGTCGTACAGATC**CCGATTCATGAGAGG. BAM5: CCCATCGGATCCGGCACAATGGCGAGGAAGTTATC. PCR of full-length LIV-1 cDNA was performed with BAM5 and M3A or M3G to produce constructs coding for proteins with seven or one TM domains respectively. Schneider S2 *Drosophila* cells were maintained in Drosophila Expression System (Invitrogen) expression medium with 10 % foetal calf serum at 24 °C in sealed flasks. Cells were transfected with the relevant LIV-1 cDNA construct using calcium phosphate transfection (Invitrogen) following the manufacturer's instructions. Briefly, 1×10^6 cells/ml were co-transfected with 19 μg of DNA and 1 μg of hygromycin-resistant plasmid (pCoHygro) before 24 h incubation. The cells were grown in hygromycin selection medium for approx. 4 weeks before testing for recombinant protein expression.

SDS/PAGE, Western analysis and deglycosylation

Transfected CHO cells were harvested at different times between 8 and 48 h. After transfection, they were lysed for 1 h in ice-cold lysis buffer [5.5 mM EDTA/0.6 % Nonidet P40/1/10 mammalian protease inhibitor cocktail (Sigma) in Krebs–Ringer Hepes buffer [24]] and immunoprecipitated with 1 μg of mouse anti-V5 antibody (Invitrogen). Cells from 10 mm × 60 mm dishes were pooled routinely for LIV-1 to compensate for the low expression levels, whereas a 1 mm × 60 mm dish was used for LacZ-expressing cells. Samples were separated by SDS/PAGE [10 % (v/v) gel] and transferred to 0.25 μm nitro-cellulose membrane (Schleicher and Schuell, London, U.K.). Control samples from CHO cells transfected with the LacZ gene (Invitrogen) were diluted 1/10 before SDS/PAGE due to the considerable increase in produced recombinant protein compared with LIV-1. Membranes were blocked with 5 % (w/v) non-fat milk in PBS and probed with anti-V5 antibody (1/5000 in 1 % non-fat milk/PBS) followed by goat anti-mouse horseradish peroxidase (1/500 in 1 % non-fat milk/PBS) and immunoreactive bands were visualized by

chemiluminescence using West Femto reagent (PerbioScience). To investigate deglycosylation, CHO cell lysate fractions expressing recombinant LIV-1 or *in vitro* translated LIV-1 were incubated with the endoglycosidase PNGase F (peptide N-glycosidase F, 2 units; Boehringer Ingelheim, Bracknell, U.K.) overnight at 37 °C before Western-blot analysis.

Fluorescence microscopy

Cells (2.2×10^5) were grown on 0.17 mm thick coverslips for 24 h before transfection. Cells were fixed with 4 % (v/v) formaldehyde for 15 min, permeabilized with or without 0.4 % saponin in PBS for 15 min, blocked with 10 % (v/v) normal goat serum, incubated with anti-V5 antibody (1/2000) for 1 h at room temperature (25 °C), Alexa Flour 488-conjugated anti-mouse antibody (1/1000; Molecular Probes, Europe BV, Leiden, The Netherlands) for 1 h and assembled on to slides using Vectorshield (Vector Laboratories, Peterborough, U.K.) with 1.5 μg/ml DAPI (4,6-diamidino-2-phenylindole) to counterstain the nucleus. All coverslips were viewed on a Leica RPE automatic microscope using a $\times$100 oil immersion lens. Fluorescent superimposed images were acquired by using a multiple band-pass filter set appropriately for DAPI, fluorescein and Texas Red as well as a bright field for DIC (differential interference contrast). To confirm that the V5 antibody was detecting recombinant LIV-1, a rabbit antiserum was produced by injecting the peptide STPPSVTSKSRVSRL (LIV-1 residues 215–229) conjugated to a multiple antigen peptide core and was incubated as above at 1/50 dilution with the anti-V5 antibody.

FACS analysis

For FACS analysis, mammalian cells, harvested carefully by pipette and resuspended in Krebs–Ringer Hepes buffer, were incubated with 50 μM Newport Green Diacetate (Molecular Probes) for 1 h at 37 °C. Addition of 25 μM zinc chloride or the zinc-specific chelator TPEN [*N*,*N*,*N*′,*N*′-tetrakis-(2-pyridylmethyl)ethylenediamine; Molecular Probes] and subsequent incubations were also at 37 °C. A Becton-Dickinson FACS III flow cytometer and software were used to analyse FACS results. Insect cells for analysis were resuspended in PBS with 1 % BSA with or without 1 % saponin. Cells were incubated on ice with anti-V5 antibody (1/50) for at least 1 h followed by fluorescein-conjugated secondary antibody for at least 30 min.

RESULTS

Tissue distribution of LIV-1

The multiple-tissue expression array (Figure 1) shows that LIV-1 is expressed in a number of different tissues with highest levels in the breast (F9), prostate (E8), placenta (B8), kidney (A7), pituitary (D3) and corpus callosum (C2). Of interest is the particularly high level of LIV-1 expression in HeLa cells (B10), which are derived from an adenocarcinoma of the cervix, and also lung carcinoma (H10). It is also evident that LIV-1 appears at lowest levels in the intestine and heart.

Computer prediction of LIV-1 secondary structure

The computer-predicted secondary structure of LIV-1 indicates a protein with 6–8 TM domains, a molecular mass of 84 kDa and a cleavable signal peptide between residues 19 and 20 (Figure 2). LIV-1 has a long extracellular N-terminus (317 residues of a total 749 amino acids) and a short extracellular C-terminus. A

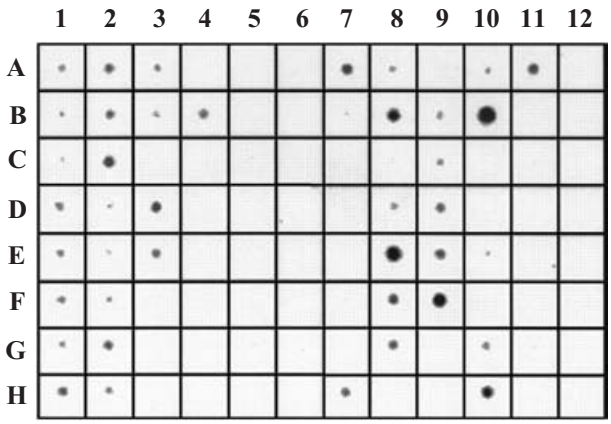

Figure 1 Tissue distribution of LIV-1

Autoradiograph of a human multi-tissue expression array hybridized with an LIV-1-specific cDNA probe. High levels of LIV-1 expression are observed in breast (F9), prostate (E8), HeLa cells (B10) and also in lung carcinoma (H10) and a number of other different tissues. Tissues represented on the human multi-tissue expression array: A1, whole brain; A2, cerebellum left; A3, substantia nigra; A4, heart; A5, oesophagus; A6, colon transverse; A7, kidney; A8, lung; A9, liver; A10, leukaemia HL-60; A11, foetal brain; A12, yeast total RNA; B1, cerebral cortex; B2, cerebellum right; B3, accumbens nucleus; B4, aorta; B5, stomach; B6, colon descending; B7, skeletal muscle; B8, placenta; B9, pancreas; B10, HeLa S3; B11, foetal heart; B12, yeast tRNA; C1, frontal lobe; C2, corpus callosum; C3, thalamus; C4, atrium left; C5, duodenum; C6, rectum; C7, spleen; C8, bladder; C9, adrenal gland; C10, leukaemia K562; C11, foetal kidney; C12, *Escherichia coli* rRNA; D1, parietal lobe; D2, amygdala; D3, pituitary gland; D4, atrium right; D5, jejunum; D6, blank; D7, thymus; D8, uterus; D9, thyroid gland; D10, leukaemia MOLT-4; D11, foetal liver; D12, *E. coli* DNA; E1, occipital lobe; E2, caudate nucleus; E3, spinal cord; E4, ventricle left; E5, ileum; E6, blank; E7, peripheral blood leucocyte; E8, prostate; E9, salivary gland; E10, Burkitt's lymphoma Raji; E11, foetal spleen; E12, poly r(A); F1, temporal lobe; F2, hippocampus; F3, blank; F4, ventricle right; F5, ileocaecum; F6, blank; F7, lymph node; F8, testis; F9, mammary gland; F10, Burkitt's lymphoma Daudi; F11, foetal thymus; F12, human C_0t-1 DNA; G1, p.g. of cerebral cortex; G2, medulla oblongata; G3, blank; G4, inter-ventricular septum; G5, appendix; G6, blank; G7, bone marrow; G8, ovary; G9, blank; G10, colorectal adenocarcinoma SW480; G11, foetal lung; G12, human DNA 100 ng; H1, pons; H2, putamen; H3, blank; H4, apex of the heart; H5, colon ascending; H6, blank; H7, trachea; H8, blank; H9, blank; H10, lung carcinoma A549; H11, blank; H12, human DNA (500 ng).

schematic of predicted structure is shown in Figure 3(A). TM IV of LIV-1 contains the same conserved histidine residue present in ZIP transporters but it is followed by asparagine in place of the serine of ZIP transporters. In place of the conserved HXXXE in TM V of ZIP transporters, LIV-1 has HEXXHE, which is highly conserved in other sequences of the LZT family. From the hydrophobicity plot (Figure 3B), it is noticeable that TMs IV and V are the least hydrophobic of the TM domains and were not predicted as TM domains by four of the six packages used. However, since they were both predicted by TMPred and DAS and they have considerable homology with TM IV and V of ZIP transporters [5], they have been included. The motif (HEX**P**H**E**XGD) at residues 629–637 fits the consensus sequence for the catalytic zinc-binding-site motif of the zincin and peptide deformylase groups of metalloproteases [25–27] and is predicted to be situated within TM V [5]. The LIV-1 sequence contains a significantly high proportion of histidine residues, greater than the 99 % quantile point [17]. These histidine-rich areas include five simple tandem repeats, HHSDHE, at the N-terminus, the extracellular loop between TMs II and III and the intracellular loop between TMs III and IV (Figure 3A and Table 1).

Expression of recombinant LIV-1 protein *in vitro* and in CHO cells

The LIV-1 cDNA (U41060) was cloned into the expression vector pcDNA3.1/V5-His-TOPO to enable expression in mammalian

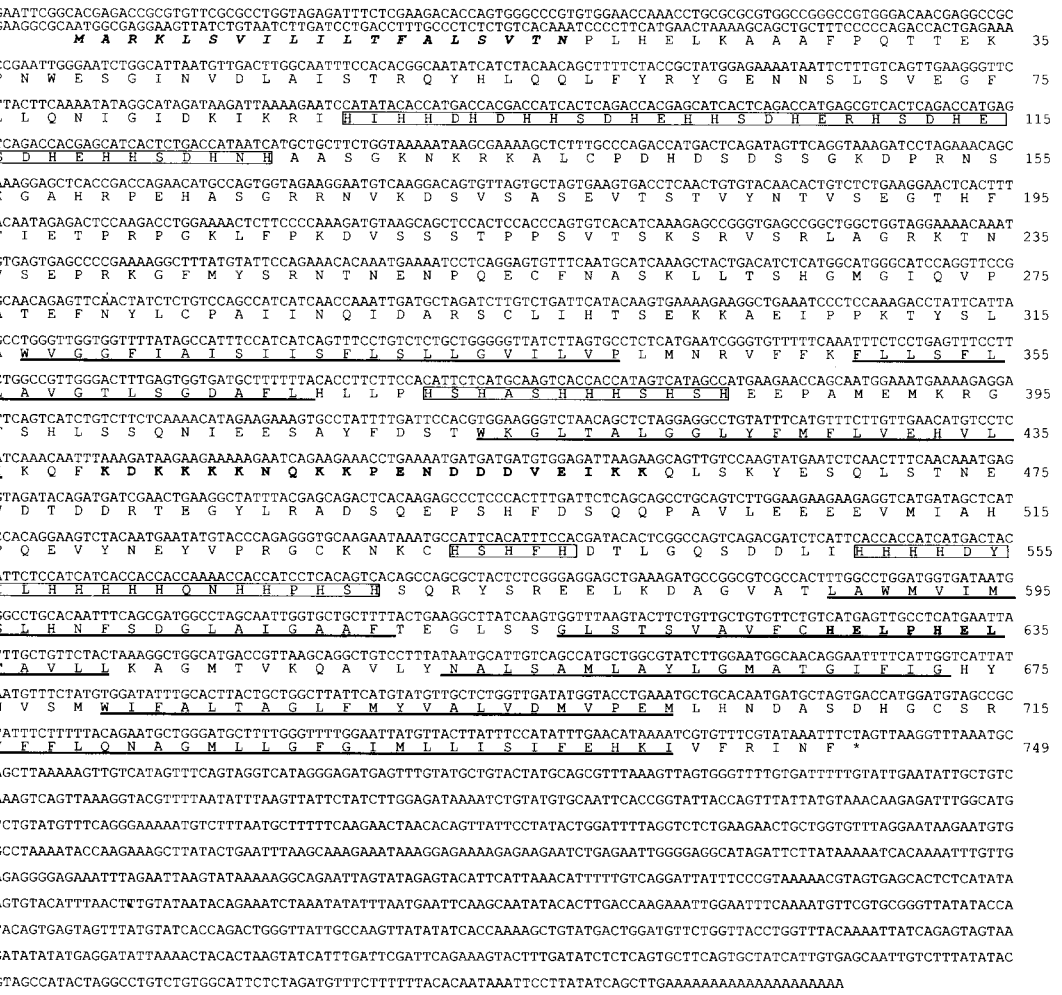

Figure 2 cDNA and protein sequence of LIV-1

cDNA sequence of LIV-1 (accession no. U41060), including the predicted amino acid sequence from the open reading frame, start position 138. Potential TM domains are underlined, histidine-rich regions are boxed, signal peptide is in bold italics, catalytic metalloprotease zinc-binding site motif (residues 629–637) and mixed charge region (residues 442–462) are in boldface. Numbers on the left refer to the cDNA sequence and numbers on right refer to the amino acid sequence.

cells from the cytomegalovirus promoter. The subsequent recombinant protein was expressed as a fusion protein with a 5 kDa V5 tag on the C-terminal end, enabling detection using the anti-V5 antibody. To ascertain the optimal time post-transfection for maximum LIV-1 production, samples were harvested at different time periods between 8 and 48 h, producing optimal expression of LIV-1 at 16 h (K. M. Taylor, E. Joyce and R. I. Nicholson, unpublished work). Subsequently, the LIV-1 construct was transiently transfected into CHO cells for 16 h and the control CHO cells were transfected without DNA. To determine the size of the expressed LIV-1 protein, transfected cells were lysed and immunoprecipitated with the anti-V5 antibody to demonstrate a single band of 105 kDa for LIV-1 (Figure 4A). The addition of butyrate 14 h before harvest (lane 1) considerably increased the intensity of the LIV-1 band (lane 2). The control transfected CHO cells (lane 3) produced no such band. The lower band observed was presumed to be residual immunoglobulin from the immunoprecipitation as this was never present without immunoprecipitation. The mass of the 105 kDa band agreed with the predicted molecular mass of 84282 Da for LIV-1 and approx. 15 kDa due to post-translational modifications such as the predicted N-linked glycosylation (Table 1), taking into account the 5 kDa of the V5 C-terminal tag in this vector.

To confirm the presence of N-linked glycosylation, a LIV-1 transfected CHO cell lysate was treated with PNGase F to remove any such chains (Figure 4A, lanes 4 and 5 respectively). Lane 6 represents the control CHO cells incubated with PNGase F. This treatment produced a reduction of approx. 15 kDa in the LIV-1 band confirming N-linked glycosylation. The presence of these side chains was also verified by TNT of LIV-1, using TNT either without or with canine pancreatic microsomes (Figure 4C, lanes 1 and 2 respectively). This method produced a band of the same size for LIV-1 as well as a second lower band when microsomes were present (lane 2), suggesting incomplete post-translational modification. This band was reduced in size when either microsomes were absent (lane 1) or after treatment with PNGase F (lane 3). These results together confirm that the molecular mass of LIV-1 is expressed as a band of 100 kDa, approx. 15 kDa of which is due to the presence of N-linked glycan chains.

The LIV-1 sequence contains a PEST motif with a score of 9.07 (residues 210–223) as well as numerous motifs, which can target proteolytic degradation (Table 1), particularly a motif (residues 213–220) similar to a ubiquitin pathway degradation signal. Therefore this *in vitro* translation system was used to determine if LIV-1 was associated with ubiquitin in cells. *In vitro* translated LIV-1 without microsomes was immunoprecipitated with either

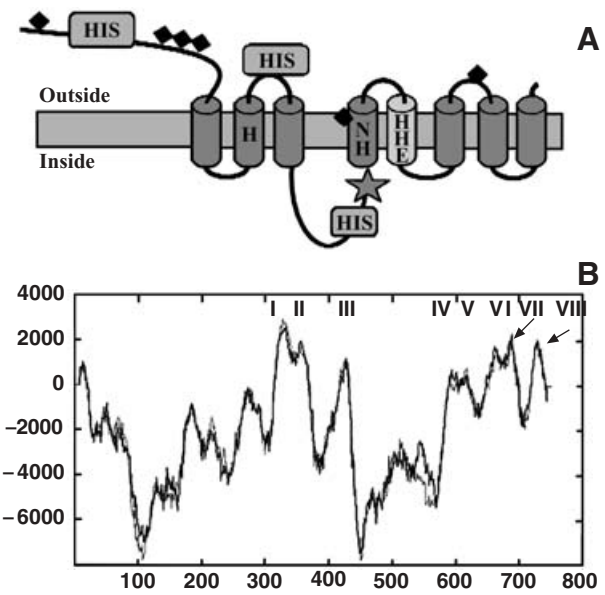

Figure 3 Secondary-structure prediction of LIV-1

(**A**) Schematic representation of LIV-1 secondary structure. Barrels, TM domains; Pale barrel, TM domain V with conserved metalloprotease (HEX**P**H**E**) motif unique to the LIV-1 subfamily; ◆, predicted N-linked glycan sites; HIS, $(HX)_n$ histidine-rich repeats; ☆, conserved mixed charge region upstream of TM IV; letters in barrels, residues conserved in the LIV-1 subfamily in positions identical or similar to those conserved in ZIP transporters, HN in TM IV and HXXHE in TM V. (**B**) Hydrophobicity plot of LIV-1 using TMPred [19] with numbers added to indicate predicted TM domains I–VIII.

anti-V5 (Figure 4C, lanes 4 and 5) or anti-ubiquitin (Figure 4C, lane 6) antibodies and subsequently analysed by Western blot and probed with the anti-V5 antibody (Figure 4C, lanes 4 and 6) or the anti-ubiquitin antibody (Figure 4C, lane 5). This demonstrated the presence of LIV-1 when either immunoprecipitated with a ubiquitin antibody (Figure 4C, lane 6) or a V5 antibody (Figure 4C, lane 5). Evidence of potentially poly-ubiquitinated LIV-1 was observed by a higher molecular-mass smear in both samples that had been exposed to the anti-ubiquitin antibody (lanes 5 and 6).

Expression of recombinant LIV-1 in Schneider S2 cells

To investigate whether the predicted membrane topology for LIV-1 was correct, Schneider S2 cells were stably transfected with constructs coding for two TM-deletion mutants of LIV-1, termed mutants A and G, where mutants A and G had seven and one TM domains respectively. If the topology prediction in Figure 3(A) is correct, these mutations are predicted to engineer proteins with the C-terminus inside the cell and hence also the V5 tag. Both recombinant proteins were successfully expressed and produced bands of the expected masses (52 and 101 kDa for mutants G and A respectively) for fully glycosylated proteins (Figure 4B, lanes 1 and 2 respectively). These were calculated assuming that the carbohydrate side chain in insect cells was 3 kDa [24] and all potential N-linked sites contained glycan chains. Mutant G, residues 1–345, was predicted to have a mass of 53 kDa that corresponded to a molecular mass of 41 kDa (including the 2.6 kDa for the V5 tag in this vector) with four potential N-linked glycan sites. Mutant A, residues 1–716, was predicted to have a mass of 101 kDa that corresponded to a molecular mass of 83 kDa (including the V5 tag) with six potential N-linked glycan sites. Also shown is the control Schneider S2 cells (lane 3) and cells transfected with the LacZ control plasmid (lane 4). The complex TM structure of LIV-1 and its association with cell membranes were confirmed by the observation that the recombinant LIV-1 protein was only detected in the cell lysis supernatant instead of the residual cell pellet after increasing the detergent concentration and time for lysis. All stable cell lines expressing the LIV-1 TM-deletion mutants showed the same staining associated with the plasma membrane when probed with V5 antibody, compared with untransfected S2 cells (K. M. Taylor, L. Hadley and R. I. Nicholson, unpublished work). The number of potential TM domains present in the protein did not alter the cell location.

The level of expression of LIV-1 protein in Schneider S2 cells was extremely low (Figure 4B). This was not due to the weak metallothionein promoter as the LacZ–V5 fusion protein control (diluted 1/100 compared with LIV-1) produced strong bands after 2 min (Figure 4B, lane 4) compared with more than 15 h for LIV-1 proteins in the same system (Figure 4B, lanes 1 and 2).

FACS analysis of cells stably expressing LIV-1 mutant G (one TM domain) or mutant A (seven TM domains) only produced increased fluorescence when cells were permeabilized (Figure 4D, grey hollow curves), which was not observed with the control

Table 1 Details of sequence motifs found in LIV-1 protein sequence

LIV-1 residue number	Sequence	Potential motif or degradation signal
3–6	RKLS	Potential endoplasmic reticulum retention signal
67, 235, 260, 277, 601, 678	NX(S,T)	N-linked glycosylation
98–103, 104–109, 110–115, 116–121 122–126	HHSDHE, HHSDHE, RHSDHE HHSDHE, HHSDH	Simple tandem histidine-rich repeat
442–462	KDKKKKNQKKPENDDDVEIKK	Mixed charge region
3, 76, 136, 232, 242 88, 135, 193, 393 304, 444, 445, 446, 450, 461 169	RK KR KK RR	Dibasic motifs as proteolysis signals [47]
86, 133, 150, 153, 162, 170, 203, 206 223, 225, 228, 304, 439, 442, 444 445, 446, 447, 460, 528, 575, 742	(R/K)X*n*(R/K) where $n = 2$, 4 or 6	Dibasic motifs recognizable by proprotein convertases [48]
210–223	KDVSSSTPPSVTSK	Strong PEST site score + 9.07 [16]
213–220	SSSTPPSV similar to SSSTDSTP	Ubiquitin degradation signal [49]

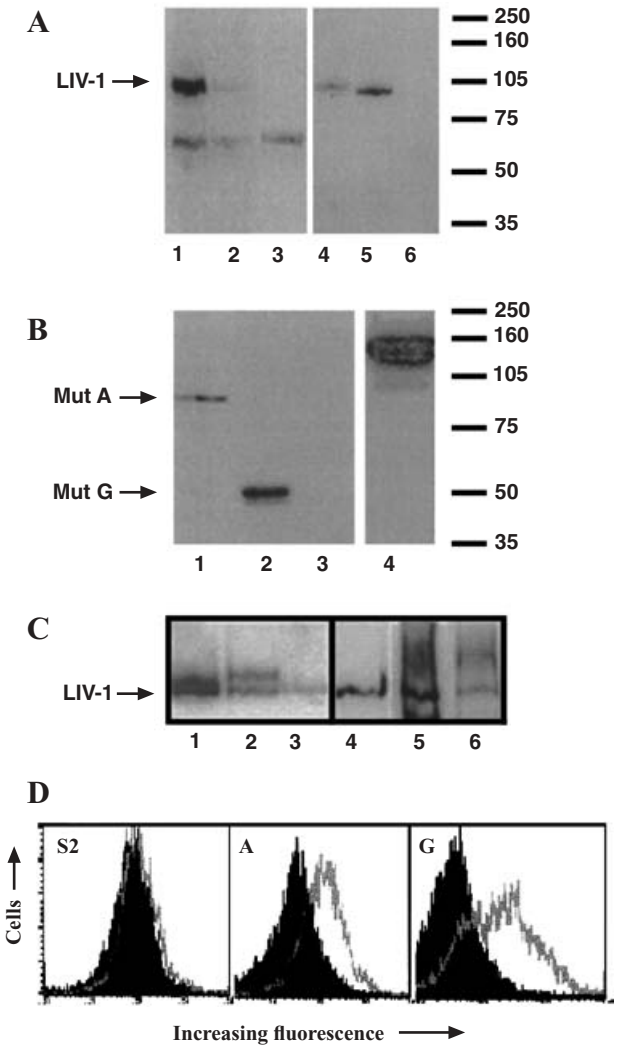

Figure 4 Western-blot analysis of recombinant LIV-1

Western-blot analysis of recombinant LIV-1 in CHO cells (**A**), insect cells (**B**) and *in vitro* (**C**). The position of the molecular-mass markers is given in kDa on the right. (**A**) Immunoprecipitation with V5 antibody of CHO cells expressing LIV-1 (lanes 1–3). LIV-1 produces a band of 105 kDa (lane 2), which is increased in intensity by sodium butyrate treatment (lane 1). Control-transfected-CHO cells produced no such band (lane 3). The LIV-1 band (lane 4) decreased in size after incubation with PNGase F (lane 5), indicating the presence of N-linked glycan chains. Lane 6 represents CHO-transfection control. (**B**) Schneider S2 insect cells stably expressing TM deletion mutant A (lane 1) with 7 TM domains or mutant G (lane 2) with 1 TM domain. Lane 3 shows the control Schneider S2 cells. The overexposed control β-galactosidase band (diluted 1/100) developed for the same time as LIV-1 is shown in lane 4. (**C**) *In vitro* translation of LIV-1 without (lane 1) or with (lane 2) canine pancreatic microsomes shows a difference in size which is abolished by incubation with PNGase F in the presence of microsomes (lane 3), confirming the presence of N-linked glycan chains. Immunoprecipitation with the anti-V5 antibody (lanes 4 and 5) or anti-ubiquitin antibody (lane 6) and probing with either anti-V5 antibody (lanes 4 and 6) or anti-ubiquitin antibody (lane 5) of *in vitro* translated LIV-1 without microsomes confirms the association of LIV-1 with ubiquitin. (**D**) FACS analysis of Schneider S2 cells expressing no recombinant protein (S2), mutant A (7 TM) or mutant G (1 TM). Black areas indicate unpermeabilized cells, grey hollow curves indicate increase in fluorescence when cells were permeabilized with saponin.

Schneider S2 cells. These results indicated the intracellular presence of the V5 tag in these constructs, suggesting that both the N- and C-termini of LIV-1 are positioned extracellularly, agreeing with the predicted topology of full-length LIV-1 in Figure 3(A).

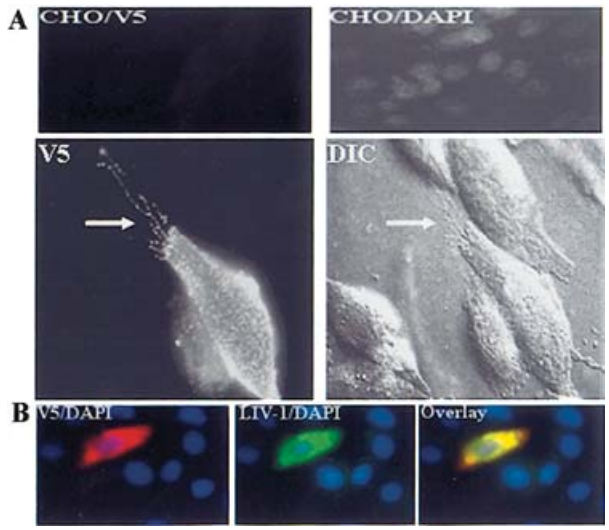

Figure 5 Fluorescence imaging of recombinant LIV-1 in CHO cells

(**A**) Fluorescence microscopy of unpermeabilized fixed CHO cells transfected with the LIV-1–V5 fusion protein, probed with the anti-V5 antibody and Alexa Fluor 488 (V5), indicates the presence of LIV-1 on the plasma membrane and lamellipodiae (arrow). DIC image of the same LIV-1–V5 expressing cells showing the plasma membrane lamellipodiae (DIC, arrow). Control-transfected CHO cells did not show any staining when probed as above (CHO/V5). The nuclei of these same cells were counterstained with DAPI to gauge the total number of cells present (CHO/DAPI). (**B**) Fluorescence microscopy of unpermeabilized fixed CHO cells transfected with the LIV-1–V5 fusion protein, probed with both the LIV-1-specific polyclonal antibody (green) conjugated to Alexa Fluor 488 (LIV-1/DAPI) and the anti-V5 antibody (red) conjugated to Alexa Fluor 594 (V5/DAPI) indicates a complete overlap of the staining pattern (Overlay, yellow). The cell nuclei are counterstained blue with DAPI.

Cellular location of recombinant LIV-1 in mammalian cells

For LIV-1 to act as a zinc influx transporter, as suggested by its similarity to ZIP transporters, it is required to reside on the plasma membrane of cells. We therefore prepared LIV-1-transfected cells on coverslips for fluorescent microscopy imaging by fixing and incubating with anti-V5 antibody followed by an Alexa-488 conjugate. This established LIV-1 localization to the plasma membrane in non-permeabilized cells (Figure 5A, V5), especially the lamellipodiae, as confirmed by DIC imaging (Figure 5A, DIC and arrows). To confirm that the V5 antibody was only staining those cells expressing LIV-1, control-mock-transfected CHO cells were also probed with the anti-V5 antibody followed by an Alexa-488 conjugate (Figure 5A, CHO/V5) and did not show any background staining. The nuclei of the cells in the same field of view were counterstained with DAPI (Figure 5A, CHO/DAPI) as an indication of cell number. To confirm that the V5 antibody was detecting only those cells expressing LIV-1, LIV-1-transfected CHO cells were probed with both the V5 antibody (Figure 5B, V5/DAPI, red) and the polyclonal LIV-1-specific antibody (Figure 5B, LIV-1/DAPI, green) in the same cells (Figure 5B, overlay, yellow). The identical staining pattern obtained validates the use of the V5 antibody to detect recombinant LIV-1.

Zinc transport

To test the hypothesis that LIV-1 was a functional member of the ZIP transporter family, we investigated zinc uptake in CHO cells expressing recombinant LIV-1 compared with control cells. Cell suspensions were loaded with the fluorescent zinc indicator Newport Green Diacetate, and the resulting basal cytosolic

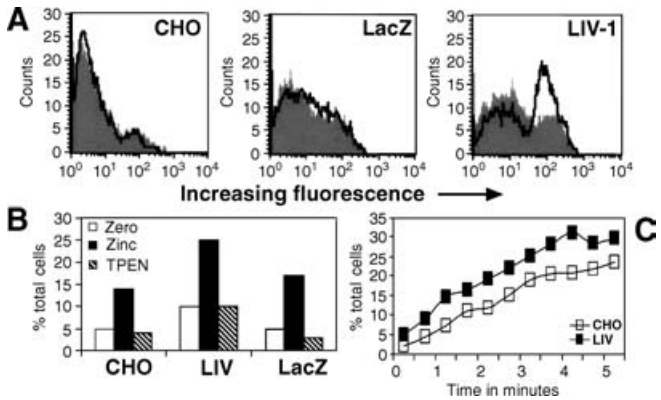

Figure 6 Zinc-transport ability of LIV-1 expressing cells

CHO cells transiently transfected with LIV-1, LacZ or no DNA (CHO) were loaded with Newport Green diacetate and fluorescence read by FACS. Each figure is a representative result of at least three experiments. (**A**) Black area represents basal reading; grey line represents 15 min treatment with 25 μM zinc. (**B**) White bars represent basal reading, black bars represent fluorescence after treatment with 25 μM zinc for 30 min, hatched bars represent subsequent treatment with 25 μM TPEN for 30 min. (**C**) Time course over 5 min of zinc influx ability of CHO cells expressing LIV-1 (closed squares) or CHO controls (open squares).

fluorescence of the cells was documented by FACS analysis. Control cells transfected with the LacZ gene (Figure 6A, grey area) showed a small increase in the basal fluorescence compared with CHO controls. This may be explained by the presence of a cytosol-located zinc-binding polyhistidine tag on the C-terminus of the cytosolic β-galactosidase recombinant protein. The same polyhistidine tag on the C-terminus of recombinant LIV-1 would be extracellular and therefore would not interfere with the intracellular fluorescence. We also investigated the ability of these cells to respond to increases in extracellular zinc by incubating them in buffer with excess zinc (25 μM) for 15 min. This exposure to 25 μM zinc had little effect on either control CHO cells (Figure 6A, black hollow curve) or those transfected with the LacZ gene (Figure 6A, black hollow curve), whereas the cells expressing LIV-1 (Figure 6A, black hollow curve) showed a dramatic increase in intracellular fluorescence in this relatively short time period. The ability of LIV-1 to transport zinc was also temperature-dependent, as these experiments, when repeated at 4 °C, did not show any cellular zinc accumulation (K. M. Taylor and R. I. Nicholson, unpublished work). This observation suggests a transporter-mediated effect rather than one caused by binding to the cell surface. To confirm that the changes in Newport Green fluorescence were due to changes in zinc concentration, we treated cells sequentially with both zinc and TPEN, a zinc-specific chelator. The fluorescence at rest for both the CHO and LacZ control cells was lower when compared with the LIV-1-transfected cells (Figure 6B, white bars), suggesting an ability of LIV-1 to act as a zinc-influx transporter. After incubation for 30 min with 25 μM zinc (Figure 6B, black bars), all cells showed an increase in fluorescence to a similar degree that was abolished by incubation with 25 μM of TPEN (Figure 6B, hatched bars).

To test whether the increased zinc accumulation in CHO cells transfected with LIV-1 was due to an initial zinc-influx rate rather than a decreased zinc-efflux activity, zinc influx was measured over a short period of time (Figure 6C). The LIV-1 expressing cells (Figure 6C, closed squares) had an increased zinc uptake rate ($>30\%$) when compared with the control cells (Figure 6C, open squares) in a time-dependent manner.

DISCUSSION

Our study on LIV-1 has enabled us to show that, first, LIV-1 is closely related to the ZIP transporters, known as zinc-influx transporters, described previously [5,8]. Secondly, LIV-1 localizes to the plasma membrane of mammalian cells, a necessary location to have a role in zinc influx. Thirdly, LIV-1 expression in cells increases the zinc-uptake ability in a time- and temperature-dependent manner. This observed zinc uptake was not related to the endogenous zinc uptake of the cells. These results are, therefore, compatible with LIV-1 having the ability to transport zinc into cells via a carrier-mediated transport process.

Our finding that LIV-1 is located on the plasma membrane with the ability to act as a zinc-influx transporter is the first demonstration of such ability of an LZT protein. This result agrees with the proposed action of hZIP4, another human LZT family member, termed as LZT-Hs5 [5], gene mutations of which have been linked to the disease acrodermatitis enteropathica, caused by deficiency of zinc uptake from the intestinal tract [28,29]. LIV-1 contains a motif (CPALLY, residues 259–298), upstream of TM I, which is uniquely present in the LZT sequences of human, mouse and monkey origin [5]. The presence of cysteine and proline residues in this motif suggests an important conserved tertiary structure. This view is supported by one of the hZIP4 gene mutations, which cause acrodermatitis enteropathica [28], a cysteine to tyrosine mutation (C309T; $Cys^{309} \rightarrow Tyr$) within this motif.

The mouse sequence ermelin (Q8R518, 505 amino acids) is virtually identical with LIV-1 and yet has been localized to the endoplasmic reticulum [30] and not to the plasma membrane. The recent appearance of the mouse sequence (Q8C145, AK028976) with 765 amino acids in the GenBank suggests that the previous ermelin sequence was lacking most of the N-terminal residues, which may account for this location. In fact, on close inspection of the ermelin DNA sequence (BM721841), another 228 residues that match Q8C145 and LIV-1 can be obtained from the next reading frame.

This result confirms both the ability of LZT sequences to transport zinc into cells and the predicted association of this new family with ZIP transporters. However, the occurrence of a fully conserved metalloprotease signature motif in the LZT family suggests that these proteins may have an additional cellular role. This motif (HEX**P**H**E**XGD) is unique to LZT sequences in that it also contains two novel residues, proline and glutamic residues (bold), previously unprecedented in these positions in any other metalloprotease motif [5,6]. It is noteworthy that the location of LIV-1 on the plasma membrane and especially the lamellipodiae (Figure 4) is identical with that of the membrane-type metalloproteinases, such as MT1-MMP [31], which also share the same HEXXH motif. MMPs cleave extracellular matrix components and have been implicated in cancer metastasis and angiogenesis. They exist as a proprotein before activation by proteolytic cleavage near the N-terminal domain, at a conserved cysteine motif, which is not present in LIV-1. However, a recognition motif for furin-like convertases (RXKR) positioned at the end of the propeptide domain is also a characteristic of these membrane-type metalloproteinases [32]. LIV-1 has two such motifs near the N-terminus (Table 1). However, we have never observed multiple bands for a recombinant LIV-1 protein and the size obtained (Figure 3B) is consistent with an uncleaved and fully glycosylated protein. Some proteases and proprotein convertases, such as furin, have been reported to be present in increased levels in cancer tissues, increasing further with the severity of cancer [33]. We suggest that, similar to conventional ZIP transporters, this potential metalloprotease motif is situated within TM V (Figures 2 and

3A) and, therefore, placed within the pore, capable of forming a metal-binding site in a manner similar to conventional ZIP transporters [34]. This is not unprecedented as a family of metalloproteases with membrane-embedded catalytic centres, termed site-2 proteases, has been discovered recently in both *Bacillus subtilis* [35] and animals [36,37]. These metalloproteases have an HEXXH motif in one TM domain which works in concert with a second conserved motif, usually containing LDG (Leu-Asp-Gly) and often NXXP residues in the adjacent TM domain. Interestingly, LIV-1 has one LDG motif in TM V and two LDG motifs (in reverse order, agreeing with the active-site motif orientation of site-2 proteases) in the adjacent TM IV containing the HEXXH motif as well as a conserved proline residue. Whether the unique metalloprotease motif in LIV-1 has protease activity is yet to be determined.

The low expression levels of the recombinant LIV-1 protein have been a consistent observation, requiring concentration of cells, immunoprecipitation and very sensitive detection methods to visualize bands by Western blot analysis. We have concluded that this effect may relate directly to the LIV-1 sequence itself as other LZT sequences [5] and the LacZ gene control (Figure 4B, lane 4) are expressed at considerably higher levels in the same systems. It is noteworthy that the encountered problem in detecting LIV-1 by Western-blot analysis is a feature shared with other zinc transporters of the ZnT efflux type. For example, ZnT3 [38], ZnT4 [39], ZnT6 [40] and ZnT7 [41] have all been difficult to observe at the protein level. Moreover, this apparent discrepancy of RNA and protein levels for ZnT6 has been suggested to be due to post-transcriptional regulation [40].

Alternatively, the observed low levels of LIV-1 may also be explained by post-translational regulation of LIV-1, possibly by degradative mechanisms. Consistent with this, we have shown an association of LIV-1 with ubiquitin (Figure 4C, lanes 4–6), a molecule responsible for targeting proteins to the 20 S proteasome degradation pathway. This pathway is the principal mechanism for degradation of regulatory proteins involved in several key cellular processes, including oncogenesis, cellular differentiation and cell-cycle control. De-regulation of this pathway can also contribute to the development of diseases such as cancer. The LIV-1 sequence contains many potential proteolytic degradation sites (Table 1), most notable of which is a strong PEST sequence present in short-lived unstable proteins [16]. PEST sequences have been shown to control the ubiquitination of regulatory short-lived proteins such as transactivator Gcn4 [42]. The potential ubiquitin degradation signal, present in LIV-1, is remarkably similar to that present in Gcn4 [43], where it is responsible for a protein half-life of 5 min. There are also numerous arginine (RR) or lysine (KK) pairs, which can act as further signals for proteolysis [44], throughout the LIV-1 sequence (Table 1). All these results together suggest that LIV-1 may be targeted to degradation by proteolysis using the ubiquitin pathway. Interestingly, the ZIP transporter Zrt1 has been shown to be ubiquitinated in cells by interaction with lysine residue, Lys^{195}, on the long cytosolic loop between TMs III and IV [45]. It is noteworthy that LIV-1 contains 15 lysine residues on this same section of sequence, which may be indicative of similar handling in cells. It will be useful to investigate the expression of LIV-1 in the presence of inhibitors of these pathways to confirm this hypothesis and potentially increase production of LIV-1.

This is the first report of LIV-1 mRNA expression in different tissue types, including brain. However, the most elevated expression was observed in the placenta, mammary gland and prostate, which are all regulated by sex steroid hormones. Noteworthy is that two cancer-related samples on the multiple-tissue array (Figure 1), namely HeLa cells (B10) and lung carcinoma (H10), are both highly positive for LIV-1. It is equally noteworthy that expression of LIV-1 is low in the gastrointestinal tract, where hZIP4, an LZT family member, predominates [28,29], suggesting tissue specificity of the LZT proteins. This result, in combination with our previous observation of increased LIV-1 expression in breast cancer cells with metastatic ability [3] suggests a role for LIV-1 in breast cancer progression. LIV-1 is not the only human ZIP transporter that has been shown to be regulated by hormones as hZIP1, and is expressed in the malignant prostate cancer cell lines, LN-CaP and PC-3, in a hormone-dependent manner [46]. This is the first report linking functional ZIP transporters with cancer progression. Whether LIV-1 is unique among the LZT subfamily in this respect has not yet been addressed.

In conclusion, the demonstration that LIV-1 can act as a zinc-influx transporter confirms its inclusion in the LZT subfamily of ZIP transporters and their ability to act as zinc-influx transporters. Localization of LIV-1 on the plasma membrane lamellipodiae, where the membrane-type metalloproteases are also positioned, and the indication that LIV-1 is a target for ubiquitin-dependent degradation, combined with the previously reported association of LIV-1 with metastatic breast cancer is an exciting result which requires further investigation to pinpoint the exact role of LIV-1 in cancer progression.

We thank Chris Green (Liverpool University, Liverpool, U.K.) for the gift of the Bluescript plasmid containing LIV-1 cDNA sequence and the Tenovus Cancer Charity for funding.

REFERENCES

1 Manning, D. L., Daly, R. J., Lord, P. G., Kelly, K. F. and Green, C. D. (1988) Effects of oestrogen on the expression of a 4.4 kb mRNA in the ZR-75-1 human breast cancer cell line. Mol. Cell. Endocrinol. **59**, 205–212
2 Manning, D. L., McClelland, R. A., Knowlden, J. M., Bryant, S., Gee, J. M., Green, C. D., Robertson, J. F., Blamey, R. W., Sutherland, R. L., Ormandy, C. J. et al. (1995) Differential expression of oestrogen regulated genes in breast cancer. Acta Oncol. **34**, 641–646
3 McClelland, R. A., Manning, D. L., Gee, J. M., Willsher, P., Robertson, J. F., Ellis, I. O., Blamey, R. W. and Nicholson, R. I. (1998) Oestrogen-regulated genes in breast cancer: association of pLIV1 with response to endocrine therapy. Br. J. Cancer **77**, 1653–1656
4 Manning, D. L., Robertson, J. F. R., Ellis, I. O., Elston, C. W., McClelland, R. A., Gee, J. M., Jones, R. J., Green, C. D., Cannon, P., Blamey, R. W. et al. (1994) Oestrogen-regulated genes in breast cancer: association of pLIV1 with lymph node involvement. Eur. J. Cancer **30**A, 675–678
5 Taylor, K. M. and Nicholson, R. I. (2003) The LZT proteins; the new LIV-1 subfamily of zinc transporters. Biochim. Biophys. Acta Biomembr. **1611**, 16–30
6 Taylor, K. M. (2000) LIV-1 breast cancer protein belongs to a new family of histidine-rich membrane proteins with potential to control intracellular Zn^{2+} homeostasis. IUBMB Life **49**, 294–253
7 Itoh, Y. and Nagase, H. (2002) Matrix metalloproteinases in cancer. Essays Biochem. **38**, 21–36
8 Gaither, L. A. and Eide, D. J. (2001) Eukaryotic zinc transporters and their regulation. Biometals **14**, 251–270
9 Gaither, L. A. and Eide, D. J. (2000) Functional expression of the human hZIP2 zinc transporter. J. Biol. Chem. **275**, 5560–5564
10 Gaither, L. A. and Eide, D. J. (2001) The human ZIP1 transporter mediates zinc uptake in human K562 erythroleukemia cells. J. Biol. Chem. **276**, 22258–22264
11 Vallee, B. L. and Auld, D. S. (1990) Zinc coordination, function, and structure of zinc enzymes and other proteins. Biochemistry **29**, 5647–5659
12 Vallee, B. L. and Falchuk, K. H. (1993) The biochemical basis of zinc physiology. Physiol. Rev. **73**, 79–118
13 Truong-Tran, A. Q., Carter, J., Ruffin, R. E. and Zalewski, P. D. (2001) The role of zinc in caspase activation and apoptotic cell death. Biometals **14**, 315–330
14 Koh, J. Y., Suh, S. W., Gwag, B. J., He, Y. Y., Hsu, C. Y. and Choi, D. W. (1996) The role of zinc in selective neuronal death after transient global cerebral ischemia. Science **272**, 1013–1016
15 Nielsen, H., Engelbrecht, J., Brunak, S. and von Heijne, G. (1997) Identification of prokaryotic and eukaryotic signal peptides and prediction of their cleavage sites. Protein Eng. **10**, 1–6
16 Rodgers, S., Wells, R. and Rechsteiner, M. (1986) Amino acid sequences common to rapidly degraded proteins: the PEST hypothesis. Science **234**, 364–368

17 Brendel, V., Bucher, P., Nourbakhsh, I., Blaisdell, B. E. and Karlin, S. (1992) Methods and algorithms for statistical analysis of protein sequences. Proc. Natl. Acad. Sci. U.S.A. **89**, 2002–2006
18 Hirokawa, T., Boon-Chieng, S. and Mitaku, S. (1998) SOSUI: classification and secondary structure prediction system for membrane proteins. Bioinformatics **14**, 378–379
19 Hofmann, K. and Stoffel, W. (1993) TMbase – a database of membrane spanning proteins segments. Biol. Chem. Hoppe-Seyler **347**, 166–172
20 Geourjon, C. and Deléage, G. (1995) SOPMA: significant improvement in protein secondary structure prediction by consensus prediction from multiple alignments. Cabios **11**, 681–684
21 Tusnády, G. E. and Simon, I. (1998) Principles governing amino acid composition of integral membrane proteins: applications to topology prediction. J. Mol. Biol. **283**, 489–506
22 Cserzo, M., Wallin, E., Simon, I., von Heijne, G. and Elofsson, A. (1997) Prediction of transmembrane α-helices in prokaryotic membrane proteins: the dense alignment surface method. Protein Eng. **10**, 673–676
23 Nakai, K. and Horton, P. (1999) PSORT: a program for detecting the sorting signals of proteins and predicting their subcellular localization. Trends Biochem. Sci. **24**, 34–35
24 Taylor, K. M., Trimby, A. R. and Campbell, A. K. (1997) Mutation of recombinant complement component C9 reveals the significance of the N-terminal region for polymerisation. Immunology **91**, 20–27
25 Hooper, N. M. (1994) Families of zinc metalloproteases. FEBS Lett. **354**, 1–6
26 Jiang, W. and Bond, J. S. (1992) Families of metallopeptidases and their relationships. FEBS Lett. **312**, 112–114
27 Ragusa, S., Mouchet, P., Lazennec, C., Dive, V. and Meinnel, T. (1999) Substrate recognition and selectivity of peptide deformylase. Similarities and differences with metzincins and thermolysin. J. Mol. Biol. **289**, 1445–1457
28 Wang, K., Zhou, B., Kuo, Y. M., Zemansky, J. and Gitschier, J. (2002) A novel member of a zinc transporter family is defective in acrodermatitis enteropathica. Am. J. Hum. Genet. **71**, 66–73
29 Kury, S., Drenom, B., Bezieau, S., Giraudet, S., Kharfi, M., Kamoun, R. and Moisan, J. P. (2002) Identification of SLC39A4, a gene involved in acrodermatitis enteropathica. Nat. Genet. **31**, 239–240
30 Suzuki, A. and Endo, T. (2002) Ermelin, an endoplasmic reticulum transmembrane protein, contains the novel HELP domain conserved in eukaryotes. Gene **284**, 31–40
31 Chen, W. T. and Wang, J. Y. (1999) Specialized surface protrusions of invasive cells, invadopodia and lamellipodia, have differential MT1-MMP, MMP-2, and TIMP-2 localization. Ann. N. Y. Acad. Sci. **878**, 361–371
32 Nakayama, K. (1997) Furin: a mammalian subtilisin/Kex2p-like endoprotease involved in processing of a wide variety of precursor proteins. Biochem. J. **327**, 625–635
33 Thomas, G. (2002) Furin at the cutting edge: from protein traffic to embryogenesis and disease. Nat. Rev. Mol. Cell Biol. **3**, 753–766
34 Eng, B. H., Guerinot, M. L., Eide, D. and Saier, Jr, M. H. (1998) Sequence analyses and phylogenetic characterization of the ZIP family of metal ion transport proteins. J. Membr. Biol. **166**, 1–7
35 Urban, S. and Freeman, M. (2002) Intramembrane proteolysis controls diverse signalling pathways throughout evolution. Curr. Opin. Genet. Dev. **12**, 512–518
36 Weihofen, A. and Martoglio, B. (2003) Intramembrane-cleaving proteases: controlled liberation of proteins and bioactive peptides. Trends Cell Biol. **13**, 71–78
37 Rudner, D. Z., Fawcett, P. and Losick, R. (1999) A family of membrane-embedded metalloproteases involved in regulated proteolysis of membrane-associated transcription factors. Proc. Natl. Acad. Sci. U.S.A. **96**, 14765–14770
38 Palmiter, R. D., Cole, T. B., Quaife, C. J. and Findley, S. D. (1996) ZnT-3, a putative transporter of zinc into synaptic vesicles. Proc. Natl. Acad. Sci. U.S.A. **93**, 14934–14939
39 Huang, L. and Gitschier, J. (1997) A novel gene involved in zinc transport is deficient in the lethal milk mouse. Nat. Genet. **17**, 292–295
40 Huang, L. P., Kirschke, C. P. and Gitschier, J. (2002) Functional characterization of a novel mammalian zinc transporter, ZnT6. J. Biol. Chem. **277**, 26389–26395
41 Kirschke, C. P. and Huang, L. (2003) ZnT7, a novel mammalian zinc transporter, accumulates zinc in the Golgi apparatus. J. Biol. Chem. **278**, 4096–4102
42 Kornitzer, D., Raboy, B., Kulka, R. G. and Fink, G. R. (1994) Regulated degradation of the transcription factor Gcn4. EMBO J. **13**, 6021–6030
43 Varshavsky, A. (1997) The ubiquitin system. Trends Biochem. Sci. **22**, 383–387
44 Gomes, A. V. and Barnes, J. A. (1995) Pest sequences in EF-hand calcium-binding proteins. Biochem. Mol. Biol. Int. **37**, 853–860
45 Gitan, R. S. and Eide, D. J. (2000) Zinc-regulated ubiquitin conjugation signals endocytosis of the yeast ZRT1 zinc transporter. Biochem. J. **346**, 329–336
46 Costello, L. C., Liu, Y., Zou, J. and Franklin, R. B. (1999) Evidence for a zinc uptake transporter in human prostate cancer cells which is regulated by prolactin and testosterone. J. Biol. Chem. **274**, 17499–17504
47 Molloy, S. S., Anderson, E. D., Jean, F. and Thomas, G. (1999) Bi-cycling the furin pathway: from TGN localization to pathogen activation and embryogenesis. Trends Cell Biol. **9**, 28–35
48 Seidah, N. G. and Chretien, M. (1999) Proprotein and prohormone convertases: a family of subtilases generating diverse bioactive polypeptides. Brain Res. **848**, 45–62
49 Varshavsky, A. (1997) The ubiquitin system. Trends Biochem. Sci. **22**, 383–387

Received 28 March 2003/24 June 2003; accepted 2 July 2003
Published as BJ Immediate Publication 2 July 2003, DOI 10.1042/BJ20030478